Macromolecules

pubs.acs.org/Macromolecules Article

Zwitterionization of Tertiary Amines in Nanoporous Block Copolymers: toward Fouling-Resistant Ultrafiltration Membranes

Chenxu Zhang, Jiemei Zhou,* Xiangyue Ye, Zhuo Li, and Yong Wang*

Cite This: *Macromolecules* 2021, 54, 4236–4245 Read Online

ACCESS | Metrics & More | Article Recommendations | Supporting Information

ABSTRACT: Zwitterionization has emerged as a highly efficient strategy to diminish protein adsorption on separation membranes, and there is a strong need to develop new zwitterionic polymers for the preparation of nonfouling membranes. Herein, by the in situ formation of newly discovered trimethylamine *N*-oxide-derived zwitterionic polymers (PTMAO) on the surface of nanoporous block copolymers, we obtain ultrafiltration membranes exhibiting superior fouling resistance. Nanoporous membranes of (2-dimethylaminoethyl methacrylate)-*block*-polystyrene (PDMAEMA-*b*-PS) are prepared by selective swelling-induced pore generation, which are subsequently soaked in H_2O_2 to oxidize the tertiary amine groups of PDMAEMA to form zwitterionic trimethylamine *N*-oxides. This oxidation takes place fast, and >70% conversion is achieved within 30 min. The thus-zwitterionized membranes exhibit strongly enhanced hydrophilicity and flexibly tunable permselectivity. Importantly, the membranes showed ultralow protein adsorption and exceptional fouling resistance, outperforming other membranes. This work demonstrates the high efficiency of PTMAO zwitterionization in mitigating membrane fouling and provides a new approach to prepare fouling-resistant membranes.

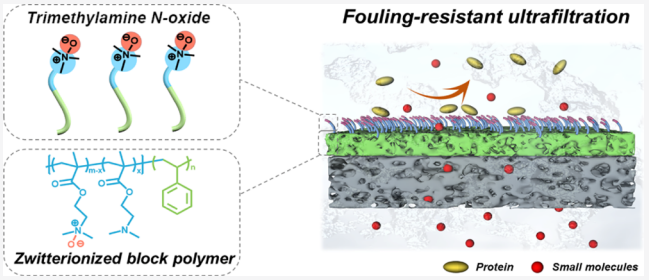

1. INTRODUCTION

Membrane separation plays an increasingly important role in providing clean water as it has being extensively used in seawater desalination, purification of surface water, and wastewater treatment.[1,2] However, foulants in the source water will inevitably result in membrane fouling, which not only significantly reduces water permeability but also threatens the continuous operation of the separation process.[3] Membrane fouling mainly originates from the nonspecific adhesion and attachment of proteins, bacteria, and cells on the membrane surface.[4,5] A systematic study on the design of antifouling membranes has been made to address this prevalent issue. One strategy is to anchor catalytic nanomaterials onto the membrane surface to achieve active antifouling, for example, by in situ immobilization of Ag or Au nanoparticles and atomic layer deposition of TiO_2.[6,7] Adhesive biofoulants can detach from membrane surfaces because of the degradation of foulants under the influence of the catalytic active reaction. The other strategy of antifouling, which is in a passive way, is designed to weaken the interaction between the foulants and membranes to avoid adhesion. The empirical "Whitesides rules" have been proposed to describe the characteristics of protein-resistant materials.[8] According to these rules, material surfaces with enhanced hydrophilicity, more hydrogen-bond acceptors, electric neutrality, and without hydrogen bond donors are expected to show better antifouling properties.[9−11] Following these guidelines, various antifouling materials were developed and anchored to the substrate surfaces by chemical immobilization or physical adhesion.[12,13] Among them, zwitterionic polymers, containing a positive charge and a negative charge in the same pendant group while exhibiting an overall neutral charge, have been demonstrated to show excellent antifouling properties.[14,15] In addition, zwitterionic polymers typically have good chemical stability and will not easily degrade with long-term usage.[16] Consequently, a long-lasting interest has aroused to render a strong fouling resistance to membranes by incorporating zwitterionic polymers onto the membrane surfaces. Three types of zwitterionic polymers, that is, poly(sulfobetaine) (PSB), poly(carboxybetaine), and poly(phosphorylcholine), have been synthesized and used as antifouling enablers to prepare fouling-resistant membranes.[17−19] The two opposite charges in zwitterions are usually linked by methylene groups, and the distance between the opposite charges, termed the carbon spacer length (CSL), is demonstrated to affect the hydration capacity of zwitterions.[20] It has been found that the charged groups in zwitterions with a short CSL are less charged, and the hydration capacity along with the nonfouling

Received: February 9, 2021
Revised: March 26, 2021
Published: April 19, 2021

https://doi.org/10.1021/acs.macromol.1c00307
Macromolecules 2021, 54, 4236–4245

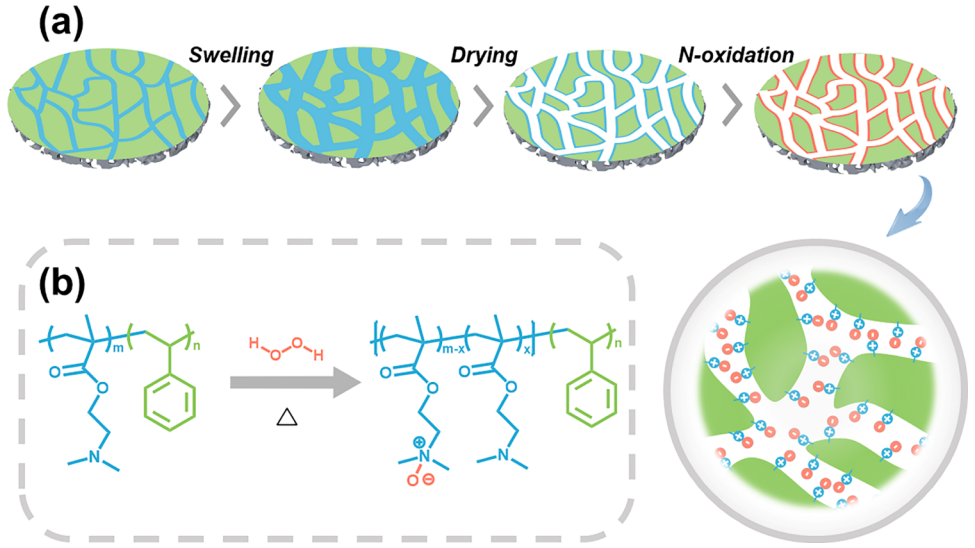

Figure 1. (a) Schematic illustration of the membrane preparation processes involving selective swelling and oxidation by H_2O_2. (b) Reaction mechanism between PDMAEMA-*b*-PS and H_2O_2.

performance of zwitterionic polymers strengthens as CSL decreases.[21] Furthermore, Jiang et al. reported that the trimethylamine *N*-oxide-derived polymer (PTMAO) presented superior hydrophilicity and nonfouling properties due to the absence of spacers between the opposite charges, and the PTMAO-coated surface exhibited ultralow protein adsorption and minimal immunogenicity, outperforming other zwitterionic polymers.[22]

Considering the unprecedented resistance to protein adsorption and easy synthesis of this emergent polyzwitterion, PTMAO, we anticipate that membranes with surfaces tethered with PTMAO will deliver exceptional fouling resistance. In this work, we realize the preparation of PTMAO-zwitterionized ultrafiltration membranes for the first time and prove that such membranes indeed show ultralow protein adsorption and consequently very strong antifouling properties. To develop zwitterionic membranes, chemical grafting and physical blending are the commonly used approaches to anchor zwitterionic chains on membrane surfaces.[23] However, the method of physical blending frequently suffers from the problem of poor adhesion, which may lead to leaching out of the zwitterionic chains during usage.[24] Instead, chemical grafting typically requires tedious pretreatments and/or generates troublesome byproducts and wastes.[25] Our group has developed an alternative route to prepare membranes with good fouling resistance on the basis of a facile strategy of selective swelling-induced pore generation.[26] Simply immersing amphiphilic block copolymers (BCPs) into a selective solvent to the hydrophilic blocks for a certain duration followed by drying enables the formation of UF membranes. Simultaneously, the hydrophilic blocks of BCPs migrate toward the membrane surface and pore walls, resulting in inborn surface hydrophilicity and fouling resistance.[27,28] Antifouling membranes prepared by selective swelling of PEG-containing BCPs including polysulfone-*block*-poly(ethylene glycol) and polystyrene-*block*-poly(ethylene oxide) have been reported in our previous studies.[29−31] PSB-zwitterionized BCP membranes were also prepared by the selective swelling of poly(2-dimethylaminoethyl methacrylate)-*block*-polystyrene (PDMAEMA-*b*-PS), with 1,3-propane sultone as the zwitterionic agent.[32] In the present work, by using the selective swelling strategy, we first prepared PDMAEMA-*b*-PS UF membranes with PDMAEMA chains containing tertiary amine groups covered along the surface and pore walls and then soaked the membranes in H_2O_2 to initiate the oxidation (Figure 1a). PDMAEMA enriched on the membrane surface can be transformed into PTMAO under in situ oxidation of tertiary amines, forming the PTMAO-zwitterionized membranes (Figure 1b). The thus-prepared membranes demonstrated outstanding fouling resistance as expected because of the nonfouling properties of PTMAO.

2. EXPERIMENTAL SECTION

2.1. Materials. The PDMAEMA homopolymer (M_n = 20.8 kDa, PDI = 1.15) and PDMAEMA-*b*-PS BCP (M_n(PDMAEMA) = 20.8 kDa, M_n(PS) = 60 kDa, PDI = 1.26) were synthesized by the method of reversible addition fragmentation chain transfer according to our previous work.[33] Silicon wafers and polyvinylidene fluoride (PVDF) porous membranes with a nominal pore size of 0.22 μm (Millipore) were used as substrates to prepare BCP thin films and composite membranes, respectively. Bovine serum albumin (BSA, molecular weight of ∼67 kDa) and lysozyme (molecular weight of ∼14.3 kDa) were obtained from Aladdin and Sigma-Aldrich, respectively. Deionized water (conductivity: 8−20 $\mu s \cdot cm^{-1}$) was used in all experiments. All other chemicals and reagents including H_2O_2 (30 wt %), ethanol (>99.7%), dichloromethane (>99.5%), chloroform (>99.5%), and tetrahydrofuran (>90%) were provided by local suppliers and used as received.

2.2. Zwitterionization of PDMAEMA Homopolymer by H_2O_2 Oxidation. PDMAEMA homopolymer (500 mg) was dissolved in deionized water (8 g) and then the H_2O_2 aqueous solution (2 g, 2 mol/L) was added dropwise under agitation (500 rpm) to initiate the oxidation of the tertiary amine groups in PDMAEMA, thus zwitterionizing PDMAEMA. The reaction was carried out at 60 °C for 10 h. Afterward, the reaction solution was dialyzed (M_w cutoff, 3.5 kDa) against deionized water for 24 h to remove residual H_2O_2. Finally, the solid oxidized polymer was obtained by freeze-drying.

2.3. Zwitterionization of PDMAEMA-*b*-PS Thin Films. PDMAEMA-*b*-PS was dissolved in chloroform with a concentration of 2 wt %. Any big aggregates or impurities were removed by filtrating the BCP solution through polytetrafluoroethylene filters with a nominal pore size of 0.22 μm three times. Afterward, the as-obtained solution was spin-coated at 2000 rpm for 30 s onto silicon substrates to prepare dense films. After being dried at 60 °C, the coated films were immersed in ethanol at 65 °C for different durations to produce

https://doi.org/10.1021/acs.macromol.1c00307
Macromolecules 2021, 54, 4236−4245

pores in the films. The films were then taken out from ethanol and dried at room temperature. Then, the swelling-treated films were soaked in a H_2O_2 aqueous solution (2 mol/L, 10 mL) at 60 °C to zwitterionize PDMAEMA blocks in the films. After the desired duration, the films were taken out from the H_2O_2 solution, then rinsed with deionized water three times, and dried at room temperature to obtain PTMAO-zwitterionized films.

2.4. Preparation of Zwitterionized PDMAEMA-*b*-PS Membranes. To prepare zwitterionized PDMAEMA-*b*-PS membranes, macroporous PVDF substrates were immersed in deionized water for 30 min to fill the macropores with water. After being withdrawn from water, the PVDF substrates were wiped with a filter paper to remove redundant water on the surface. Then, the BCP solution was spin-coated onto the water-filled PVDF substrates at 2000 rpm for 30 s. The BCP-coated PVDF membranes were heated at 60 °C for 20 min to evaporate the remaining chloroform. Afterward, the membranes were soaked in ethanol at 65 °C and then soaked in H_2O_2 solution at 60 °C to produce pores and to zwitterionize PDMAEMA, respectively.

2.5. Characterization. The surface and cross-sectional morphologies of the samples were examined using a field emission scanning electron microscope (Hitachi S4800) under an accelerating voltage of 5 kV. For cross-sectional observation, the samples were prepared by immersing in liquid nitrogen and quickly fracturing to expose the cross sections. All scanning electron microscopy (SEM) samples were coated with a thin layer of platinum to improve the conductivity before SEM characterization. At least 100 pores on the surface SEM images of each sample were measured to estimate the average pore sizes by using software Nanomeasurer. The surface elemental analysis and chemical compositions of BCP films were determined with an X-ray photoelectron spectrometer (XPS, K-alpha, Thermo Fisher). The characterization of the polymer structure was performed on a nuclear magnetic resonance spectrometer (NMR, AV400, Bruker) using D_2O as the solvent. The chemical compositions of the samples were recorded by Fourier transform infrared spectroscopy (Nicolet 8700 FT-IR spectrometer, Thermo Scientific) in the attenuated total reflection (ATR) mode. The surface hydrophilicity of BCP films supported on silicon substrates was evaluated by testing the static water contact angles (WCAs) using a contact angle goniometer (Dropmeter A100, Maist). At least three positions on each film were recorded, and the average value was reported. The thicknesses and refractive indices of BCP films were determined via a spectroscopic ellipsometer (Complete EASE M-2000U, J. A. Woollam) with an incident angle of 70°. The surface potentials of BCP membranes supported on PVDF substrates were examined by an electrokinetic analyzer (SurPASS Anton Paar, Austria).

2.6. Filtration Tests. The separation performances of composite membranes were measured using a dead-end filtration module (Amicon8003, Millipore). Prior to testing, the precompaction of each membrane was performed for 10 min under a pressure of 0.5 bar. The water volume passing through the membrane was measured, and the permeance (Perm) was calculated using eq 1

$$\text{Perm} = \frac{V}{A \cdot t \cdot p} \tag{1}$$

where V (L) is the volume of water passing through the membranes, A (m^2) is the active membrane area, t (h) is the filtering time, and p (bar) is the transmembrane pressure.

The BSA aqueous solution (0.5 g/L, pH = 7.4) was prepared by dissolving BSA in a phosphate-buffered saline (PBS) solution for the retention test. BSA concentrations of the feed and permeation solution were determined using a UV−vis absorption spectrometer (NanoDrop 2000C, Thermo Fisher) at 280 nm. The BSA rejection is calculated using eq 2

$$R = \frac{C_f - C_p}{C_f} \times 100\% \tag{2}$$

where C_f and C_p are the BSA concentration (g/L) in the feed and permeation solution, respectively.

2.7. Antifouling Tests. To evaluate the antifouling performance of the prepared membranes, the static adsorption (SA) and dynamic filtration fouling tests were executed. For the SA experiment, BSA (1 g/L) and lysozyme (1 g/L) were chosen as protein foulants to evaluate the adsorption capacity. The membranes with an area of 5.4 cm^2 were immersed in a 5 mL BSA or lysozyme solution to conduct protein adsorption. The adsorption tests lasted for 24 h at room temperature to achieve adsorption equilibrium. The protein concentration after adsorption was determined by UV−vis spectrometry, and the SA capacity of each membrane was calculated using eq 3

$$\text{SA} = \frac{(C_b - C_a) \times V}{A} \tag{3}$$

where C_b and C_a are the protein concentrations (g/L) in the solution before and after the adsorption test, respectively, V is the volume of the protein solution (mL), and A is the membrane area (cm^2).

For the dynamic fouling tests, BSA (1 g/L) was chosen as a model foulant. Deionized water and the BSA solution were filtrated alternately through the membranes for three cycles in the dead-end filtration module under a constant pressure of 0.5 bar. The initial stable water permeance of the membrane was denoted as J_0, and the BSA solution permeance of the membrane in each cycle was recorded as J_P. After each cycle of fouling, the membrane was washed by deionized water three times to remove the foulants, and the recovery water permeance in each cycle was recorded as J_R. The water flux recovery ratio (FRR), the reversible fouling ratio (R_r), the irreversible fouling ratio (R_{ir}), and the total fouling ratio (R_t) were calculated using eqs 4−7

$$\text{FRR} = \frac{J_R}{J_0} \times 100\% \tag{4}$$

$$R_{ir} = \frac{J_0 - J_R}{J_0} \times 100\% \tag{5}$$

$$R_r = \frac{J_R - J_P}{J_0} \times 100\% \tag{6}$$

$$R_t = R_{ir} + R_r \tag{7}$$

3. RESULTS AND DISCUSSION

3.1. Feasibility of Zwitterionization of PDMAEMA by H_2O_2 Oxidation. The strategy to prepare PTMAO-zwitterionized membranes in this work typically includes two processes: selective swelling of PDMAEMA-*b*-PS, which has previously demonstrated to be able to produce UF membranes with pores lined with PDMAEMA chains,[33] and the zwitterionization of PDMAEMA by H_2O_2 oxidation. First, to verify the feasibility of this H_2O_2-enabled zwitterionization of PDMAEMA, the chemical structure of the PDMAEMA homopolymer before and after H_2O_2 treatment was monitored by ^{1}H NMR. It should be noted that the PDMAEMA homopolymer, instead of the membrane-forming PDMAEMA-*b*-PS copolymer, was used here because there is no available solvent to dissolve the zwitterionized BCP for ^{1}H NMR. As shown in Figure 2a, the signals of methyl protons adjacent to nitrogen (a), methylene protons adjacent to nitrogen (b), and ester methylene protons (c) in PDMAEMA appeared at 2.2, 2.6, and 4.0 ppm, respectively.[34] After H_2O_2 treatment, these signals shifted to lower fields, and new peaks of the corresponding groups arose at 3.2, 3.6, and 4.4 ppm, respectively, indicating that the electron cloud densities of the corresponding protons were both decreased under the inductive effect of N^+ as an electron-withdrawing group. Meanwhile, we observed that the signal peak of ester

https://doi.org/10.1021/acs.macromol.1c00307
Macromolecules 2021, 54, 4236−4245

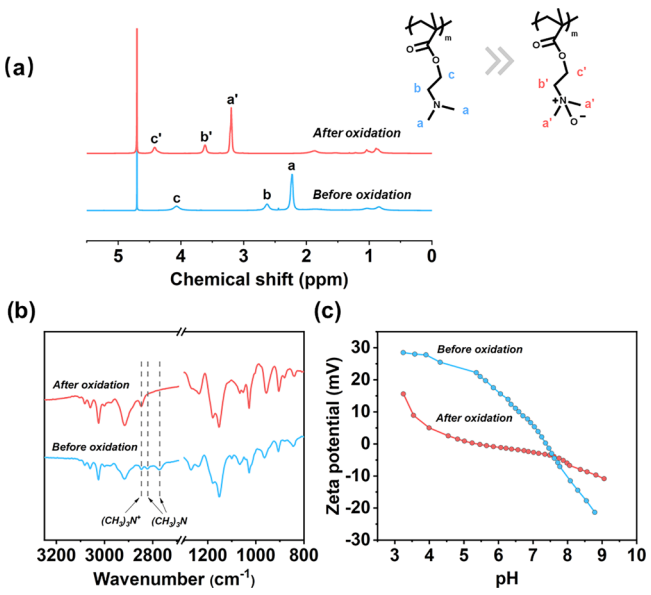

Figure 2. (a) ^{1}H NMR spectra of the PDMAEMA homopolymer before and after oxidation. (b) ATR-FTIR spectra of PDMAEMA-*b*-PS films and (c) surface zeta potentials of PDMAEMA-*b*-PS membranes before and after H_2O_2 treatment.

methylene protons (c) shifted to the left at ∼0.4 ppm, which was lower than the peak shifts of methyl (a) and methylene (b) protons adjacent to nitrogen, indicating a weaker inductive effect of N^+ on ester methylene protons due to the greater distance.

Furthermore, the chemical composition of the PDMAEMA-*b*-PS film before and after H_2O_2 treatment was also analyzed by ATR-FTIR spectroscopy (Figure 2b). The spin-coated PDMAEMA-*b*-PS film was first swelling-treated in ethanol at 65 °C for 10 h to achieve the porous structure and then immersed in a H_2O_2 aqueous solution (2 mol/L, 10 mL) at 60 °C to perform oxidation. Before H_2O_2 treatment, two characteristic peaks at 2770 and 2820 cm^{-1} corresponding to the asymmetric and symmetric stretching vibrations of tertiary amine groups were observed.[35] After oxidation, a new peak attributed to the $(CH_3)_3{-}N^+$ stretching vibration appeared at 2850 cm^{-1}. Meanwhile, both peaks at 2770 and 2820 cm^{-1} were absent. This verified the successful conversion of tertiary amines to tertiary amine *N*-oxides by the process of in situ H_2O_2 oxidation. During oxidation, tertiary amines containing lone-pair electrons can combine with atomic oxygen from H_2O_2 by forming coordinate bonds, thus producing peroxides. Peroxides which are highly unstable subsequently undergo the dewatering process, forming *N*-oxides containing the zwitterionic structure.[36]

The surface zeta potential of the PDMAEMA-*b*-PS membrane prepared by ethanol swelling was estimated under varied pHs (Figure 2c). The pristine membrane before oxidation showed positive zeta potentials, with pH ranging from 3.2 to 7.3. The initial value was 28.5 mV at the pH of 3.2, which is ascribed to the presence of PDMAEMA chains on the membrane surface. After H_2O_2 oxidation, the membrane exhibited lower zeta potentials, and the potential values were in the scope of electric neutrality (+5 to −5 mV) in the pH range of 4−8. This result confirms the neutral charging nature of the formed tertiary amine *N*-oxide groups, which is beneficial for adsorption resistance to charged proteins.

3.2. Kinetic Study of Selective Swelling and Zwitterionization of PDMAEMA-*b*-PS Thin Films. To investigate the swelling behavior of PDMAEMA-*b*-PS films, we soaked the BCP films coated on silicon substrates in ethanol at 65 °C with changing durations, followed by H_2O_2 treatment at 60 °C for 5 h. The as-coated film before swelling exhibited a smooth and dense morphology (Figure 3a). In contrast, after swelling, the film exhibited a porous structure, and the pore sizes were enlarged with prolonged swelling durations as can be clearly seen from the surface (Figure 3b−f) and cross-sectional (Figures S1 and 3g−h) SEM images. With a swelling duration of 0.5 h, some elongated pores accompanied with few round pores with an average size of ∼25 nm appeared on the film surface. When the swelling duration was increased from 2 to 5 h, more elongated pores emerged on the film surface, and the average sizes were increased to 32 and 34 nm, respectively. Further extending the swelling duration to 10 h resulted in a typical bicontinuous porous morphology, and the pore size was enlarged to 38 nm. When the swelling duration was further prolongated for 20 h, the pore morphology and size did not show noticeable changes. As the selective swelling of BCP films confined on substrates usually leads to vertical expansion, the thickness change of PDMAEMA-*b*-PS films with swelling durations monitored by ellipsometry was recorded to investigate the swelling kinetics of the BCP film. As shown in Figure 3i, the thickness of the film was rapidly increased from 210 to 267 nm in the initial swelling period of 0.5 h, and then it was gradually increased to 273 and 297 nm at the swelling durations of 2 and 5 h. Thereafter, the film remained almost unchanged in thickness. The SEM observations on the cross sections of the swelling-treated BCP films reveal that the interconnected nanoporous structure is present throughout the entire film thickness, confirming that the film thickness is increased when the swelling duration was increased to 10 h. These results suggest that the swelling of the PDMAEMA-*b*-PS films would achieve equilibrium and exhibit an interconnected nanoporous morphology at the swelling duration of 10 h. The thickness displays a total increase of about 40% because of the formation of abundant pores in the film after swelling.

We further investigate the impact of oxidation reaction on the porous structure of the films by changing the oxidation durations. The film subjected to swelling in ethanol at 65 °C for 10 h without oxidation presented an interconnected nanoporous morphology with an average pore size of 39 nm. When subjected to oxidation for various durations ranging from 0.5 to 20 h, the film did not exhibit any noticeable change in its porous morphology, and the average pore size remained nearly unchanged (Figure S2). We also investigated the thickness change of the films prepared with different oxidation durations. As shown in Figure S3, the thickness of the film before oxidation was tested to be 327 nm, and it was observed to decrease to ∼295 nm after being treated in the H_2O_2 solution for 0.5 h, and longer oxidation did not further decrease the film thickness. It should be noted that the decrement in film thickness during oxidation was about 10% of the original thickness, and it would not hurt the structural integrity of the BCP films, as demonstrated by the SEM characterization. Conversely, the thickness decrease at no expense of porosity and pore sizes is expected to reduce the mass-transfer resistance when the BCP film is employed as the separation layer, which may result in boosted permeance performance.

https://doi.org/10.1021/acs.macromol.1c00307
Macromolecules 2021, 54, 4236−4245

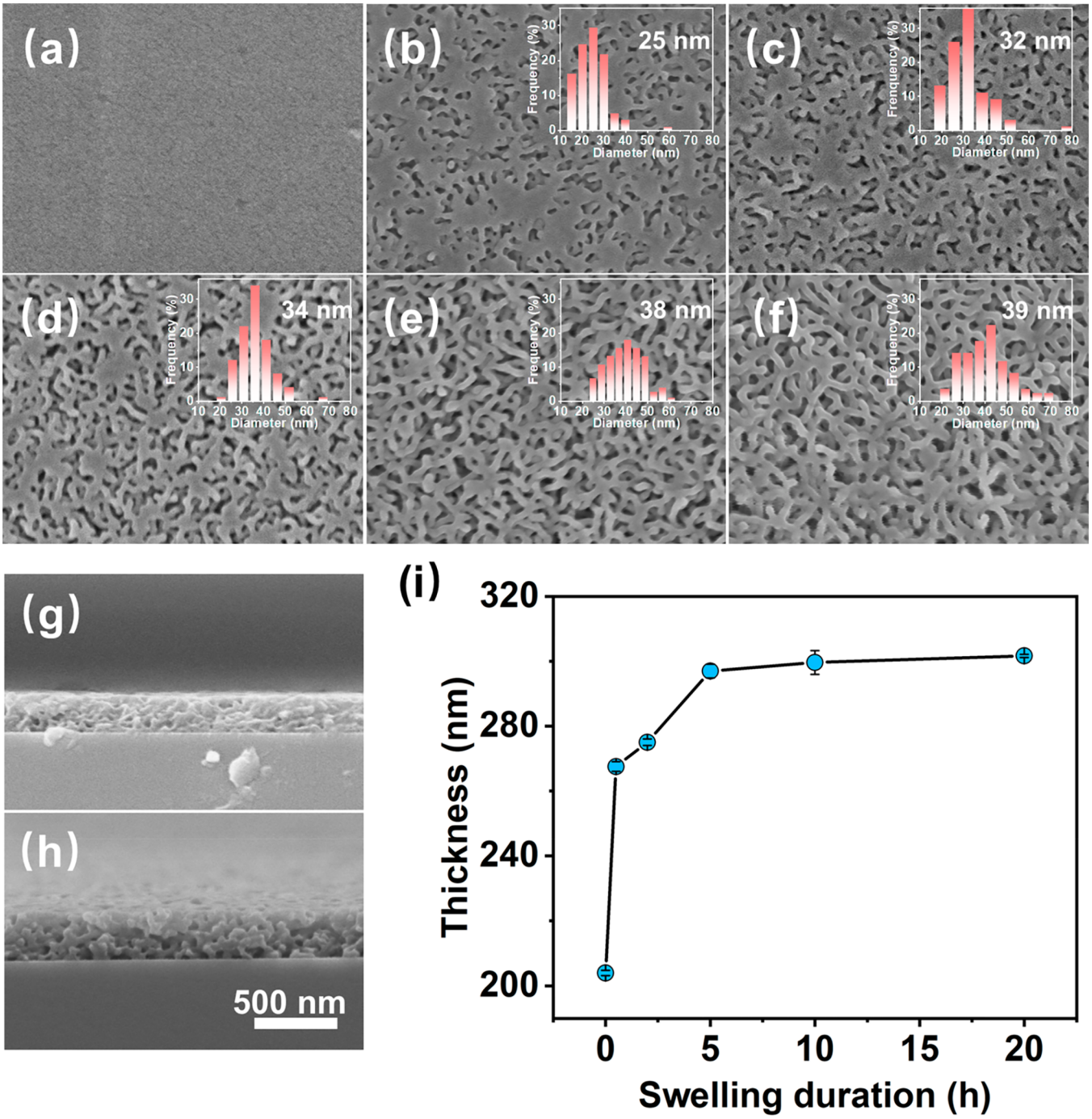

Figure 3. (a–f) Surface and (g,h) cross-sectional SEM images of the PDMAEMA-*b*-PS films subjected to swelling at 65 °C for various durations: (a) 0, (b) 0.5, (c,g) 2, (d) 5, (e) 10, and (f,h) 20 h and then oxidation at 60 °C for 5 h. Insets in (a–f) show the pore size distribution and the average pore size of the corresponding films. (i) Thicknesses of PDMAEMA-*b*-PS films for various swelling durations. All SEM images have the same magnification, and the scale bar corresponding to 500 nm is given in (h).

The change in surface hydrophilicity of the PDMAEMA-*b*-PS films subjected to H_2O_2 oxidation was investigated by the static WCA tests (Figure 4). Prior to oxidation, the BCP film after swelling in ethanol at 65 °C for 10 h showed a WCA value of 54°, which is close to that of the surface of the PDMAEMA homopolymer.[35] This can be easily understood as the PDMAEMA blocks were enriched on the film surface and pore walls after selective swelling. With H_2O_2 oxidation for various durations, a clear tendency of enhanced hydrophilicity for the BCP films was observed with the prolonged oxidation durations. The WCA value dropped rapidly to 36° in the first 2 h of oxidation, then it was gradually lowered to 29° after oxidation for 20 h. As the surface pore size and geometry of the films showed no obvious change, as observed by SEM (Figure S2), this decline in WCA values should be attributed to the formation of tertiary amine *N*-oxides that can tightly bind water molecules via electrostatic interaction and hydrogen bonding, leading to lower interfacial energy and strong surface hydrophilicity.[37]

https://doi.org/10.1021/acs.macromol.1c00307
Macromolecules 2021, 54, 4236–4245

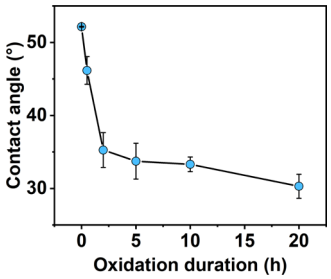

Figure 4. WCA of the PDMAEMA-*b*-PS films prepared by swelling in ethanol at 65 °C for 10 h and subsequently treated in H_2O_2 solution at 60 °C for various durations.

XPS characterization was carried out to investigate the oxidation efficiency of tertiary amines in the BCP films. As shown in Figure 5a, for the film swelling treated in ethanol at 65 °C for 10 h, only the N1s peak at 399.8 eV was present, which originated from *N* in tertiary amines. After soaking the film in the H_2O_2 solution at 60 °C for 0.5 h, a new peak located at 403 eV appeared, which should be attributed to N^+ in tertiary amine *N*-oxides.[38] This evidences the formation of zwitterions and the efficiency of this in situ oxidation strategy, which are in good agreement with other characterization results discussed above. The conversion of tertiary amine *N*-oxides can be calculated using eq 8

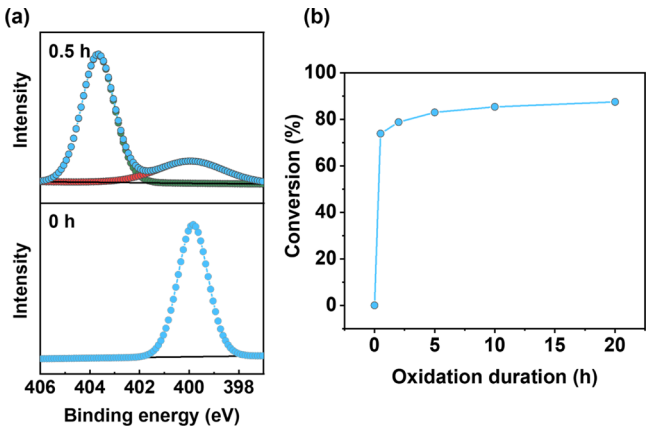

Figure 5. (a) N1s high-resolution scans of the PDMAEMA-*b*-PS films after oxidation for 0 and 0.5 h and (b) oxidation conversion of the film after oxidation for various durations.

$$\text{conv}(\%) = \frac{[N^+]}{[N^+] + [N]} \times 100\% \quad (8)$$

where [N] and $[N^+]$ represent the areas of peaks corresponding to tertiary amines and tertiary amine *N*-oxides in the XPS spectra, respectively. It can be clearly seen from Figure 5b that this in situ oxidation proceeded very fast in the initial stage as the first 0.5 h of oxidation was able to give an oxidation conversion as high as 73.9%. The oxidation rate was slowed down, as the oxidation that is prolongated for 20 h only slightly increased the conversion to 87.5%. Such a relationship between the oxidation duration and conversion is a consequence of the liquid−solid phase reaction between the H_2O_2 solution and the PDMAEMA chains tethered to the membrane pores. Upon contact of H_2O_2 and the tertiary amines in the PDMAEMA chains, oxidation took place immediately as a result of the strong activity of H_2O_2, leading to the fast conversion of tertiary amines to *N*-oxides, that is, the majority of the tertiary amines was consumed and the remaining were shielded by the newly formed *N*-oxides, requiring a longer time to react with H_2O_2 because of the retarded diffusion. Therefore, further oxidation proceeded much slowly.

3.3. Separation Performances of PTMAO-Zwitterionized Membranes. After confirming the efficient in situ oxidation of PDMAEMA-*b*-PS by H_2O_2, we prepared composite membranes with the PTMAO-zwitterionized porous BCP as the selective layers on top of macroporous PVDF substrates under varied swelling and oxidation

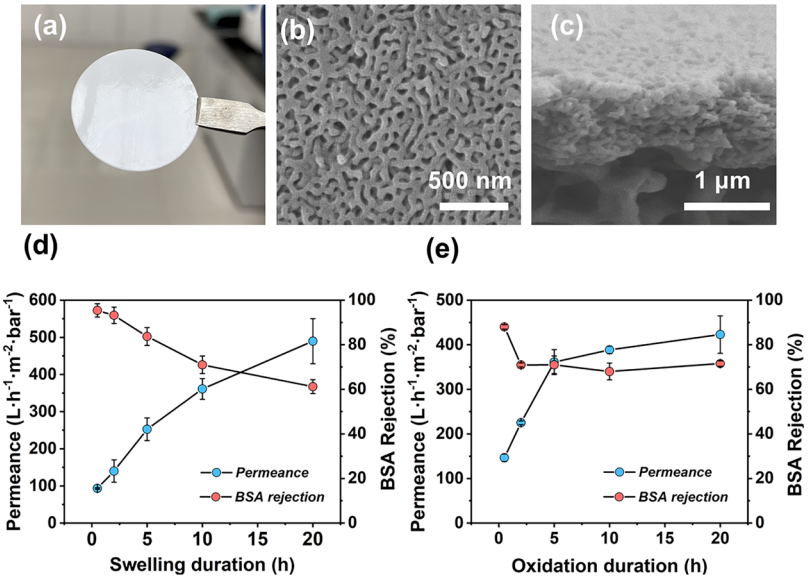

Figure 6. (a) Photograph, (b) surface, and (c) cross-sectional SEM images of the PTMAO-zwitterionized membrane. Water permeance and BSA rejections of PTMAO-zwitterionized membranes prepared with (d) different swelling durations under a fixed oxidation duration of 5 h and with (e) different oxidation durations under a fixed swelling duration of 10 h.

https://doi.org/10.1021/acs.macromol.1c00307
Macromolecules 2021, 54, 4236−4245

conditions and then investigated their separation performances. Note that the preparation of the PTMAO-zwitterionized membranes can be significantly accelerated by finishing the swelling process within 1 min through a microwave-boosted selective swelling strategy[39] and shortening the oxidation to <2 h, which can also achieve a conversion of 80%. As shown in Figure 6a, the top side of the composite membrane presented a shiny and smooth appearance, implying the thin and uniform coating of the BCP layer on the substrate. As shown in Figure 6b−c, SEM observations reveal an interconnected nanoporous morphology throughout the entire BCP layer and a bilayered composite structure of the produced membrane. Figure 6d shows the separation performances of the PTMAO-zwitterionized membranes as the function of swelling durations under a fixed oxidation duration of 5 h. Prior to swelling, the pristine membrane was confirmed to be dense and defect-free, with zero water permeance. After swelling at 65 °C for 0.5 h, the membrane exhibited a permeance of 94 L/(m^2·h·bar) and a BSA rejection of 95%, verifying that the dense BCP layer was cavitated and accessible porosity was formed. It is worth noting that the average pore size of BCP films after 0.5 h swelling was measured to be ∼25 nm, which is much bigger than that of BSA. However, a high BSA rejection could be achieved here. This is because the SEM characterization was carried out in the dry state under a high vacuum. The hydrophilic chains of PTMAO would adopt a collapsed conformation in this case, while these chains were stretched once the membrane was exposed to aqueous solutions. Therefore, the effective pore size of the membrane in use was much smaller than that measured by electron microscopy, leading to the high rejection to BSA. This has been frequently observed in membranes with the pore walls tethered with hydrophilic chains.[31,40] As the swelling duration was extended to 2 h, the membrane showed an increasing permeance of 140 L/(m^2·h·bar), and the BSA rejection was decreased to 93%. With the swelling duration further increased to 10 and 20 h, the permeance of the membrane was progressively increased to 361 and 489 L/(m^2·h·bar), with the BSA rejection decreased to 71 and 61%, respectively. On account of the same oxidation durations, the progressive increase in water permeance was due to the ever-enlarged pores and increased porosity in the BCP layer with the swelling durations. We then investigated the effect of oxidation on the permeance and rejection of membranes prepared under the same swelling condition. As shown in Figure 6e, clearly, oxidation strongly influences the permselectivity of the membrane even after a short oxidation duration. The membrane prepared with an oxidation duration of 0.5 h exhibited a permeance of 147 L/(m^2·h·bar) and a BSA rejection of 85%. With the oxidation duration extended to 2 h, the membrane showed an increased permeance of 225 L/(m^2·h·bar), and the BSA rejection was decreased to 71%. The permeances were further increased to 361, 389, and 423 L/(m^2·h·bar) as the oxidation durations were prolongated for 5, 10, and 20 h, respectively, while the BSA rejections remained stable and did not drop further. As the oxidation duration did not noticeably change the average pore sizes, the rising water permeances should be predominantly attributed to the constantly enhanced surface hydrophilicity of the PTMAO-zwitterionized BCP layers. Moreover, the decline of the BSA rejection for the membranes prepared with an oxidation duration of 2 h and less is presumably because of the change in the electric charge of the PDMAEMA chains. Before oxidation, the nanoporous layer of PDMAEMA-*b*-PS is likely to adsorb BSA because of the electrostatic interaction between the positive PDMAEMA chains and BSA molecules, partly contributing to the higher BSA rejection. After oxidation, the electrical neutrality of the generated tertiary amine *N*-oxides tethered on the membrane pores could suppress the BSA adsorption and accumulation; consequently, the BSA molecules have more chance to percolate through the pores of membranes, leading to the decreased BSA rejection. For the membranes prepared with oxidation durations that varied from 5 to 20 h, the capability to resist BSA adsorption plays a negligible role in rejecting BSA because the high degree of oxidation of tertiary amines (over 80%) has been achieved since 5 h. As a result, the membranes exhibited similar BSA rejections just because of similar pore sizes.

3.4. Antifouling Performances of PTMAO-Zwitterionized Membranes. The antifouling performances of separation membranes is usually evaluated by measuring the protein adsorption and flux recovery ability upon protein fouling.[41,42] In this study, the PTMAO-zwitterionized membrane prepared by swelling at 65 °C for 10 h and oxidation at 60 °C for 10 h was chosen to evaluate its fouling resistance. In terms of SA, BSA and lysozyme with opposite charges in PBS buffer solutions were used as the model foulants (Figure 7a). For the negatively charged protein of BSA, the PDMAEMA-*b*-PS membrane before oxidation showed a BSA adsorption of 23 μg/cm^2. By contrast, the membrane subjected to 10 h oxidation showed a significantly reduced BSA adsorption of 5.9 μg/cm^2, indicating that the PTMAO zwitterionization was able to significantly inhibit BSA protein adhesion and accumulation as a result of the charge neutrality of the PTMAO-zwitterionized surface. For the positively charged lysozyme, the membrane before PTMAO zwitterionization showed a low adsorption of 6.24 μg/cm^2 because of the electrostatic repulsion effect. Interestingly, after PTMAO zwitterionization, the membrane exhibited even lower

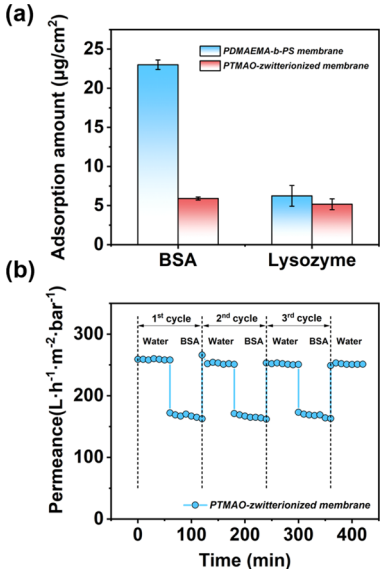

Figure 7. (a) BSA and lysozyme SA of the PDMAEMA-*b*-PS membrane prepared by swelling at 65 °C for 10 h and the corresponding PTMAO-zwitterionized composite membrane after oxidation at 60 °C for 10 h. (b) Time-dependent permeance of the PTMAO-zwitterionized membrane during alternate water/BSA filtration.

https://doi.org/10.1021/acs.macromol.1c00307
Macromolecules 2021, 54, 4236−4245

adsorption to lysozyme (5.17 $\mu g/cm^2$). Clearly, the PTMAO zwitterionization can efficiently augment the fouling resistance of membranes to both positively and negatively charged proteins due to the electric neutrality and enhanced hydrophilicity.

Dynamic fouling tests were executed to examine the flux recovery ability of the PTMAO-zwitterionized membrane using BSA as the model foulant. Figure 7b presents the time-dependent permeance of the PTMAO-zwitterionized membrane during alternate water/BSA ultrafiltration. First, deionized water was filtered through the membrane for 60 min, and the membrane showed a steady water permeance of 258 $L/(m^2 \cdot h \cdot bar)$. After continuous BSA fouling for 60 min, the BSA permeance was declined to 162 $L/(m^2 \cdot h \cdot bar)$, which should be attributed to the protein adsorption originated from intermolecular interactions and the protein deposition under pressure filtration. The recovery permeance of 251 $L/(m^2 \cdot h \cdot bar)$ was observed after the membrane was thoroughly rinsed with deionized water several times, and the FRR value was calculated to be 97%. This high FRR value demonstrates that the tertiary amine *N*-oxide groups of PTMAO can minimize the irreversible protein adsorption, while the reversible adsorption or deposition can be easily removed through water washing. After the second and third fouling cycles, the water permeance can still return to 251 $L/(m^2 \cdot h \cdot bar)$, and the FRR values had no change, indicating that the irreversible protein adsorption reached saturation in the first cycle and had no further accumulation in subsequent fouling. More details of R_t, R_r, R_{ir}, and FRR of the membrane are given in Table S1. Furthermore, we compared this PTMAO-zwitterionized membrane with other reported polymeric ultrafiltration membranes in terms of BSA SA and FRR values in dynamic filtration (Table S2) and found that our membranes exhibit excellent fouling resistance. They exhibit better FRR values and BSA adsorption than many other membranes, and their fouling resistance is close to the best performance of the reported polymeric membranes.

We note that membrane zwitterionization by PTMAO reported in this work is based on membrane discs prepared by spin coating. However, PTMAO zwitterionization is not dependent on the coating process of the BCP. In addition to thin-film composite membranes with small areas prepared by spin coating, this new zwitterionization approach by H_2O_2 oxidation of tertiary amines is expected to be applicable to large-area membranes, in the form of either flat sheets or hollow fibers, prepared by roll-to-roll coating processes for large-scale manufacturing and real-world applications.

4. CONCLUSIONS

In summary, we prepared a new type of zwitterionized membrane with exceptional fouling resistance based on newly discovered zwitterionic polymers of trimethylamine *N*-oxides (PTMAO). We first demonstrated that PDMAEMA homopolymers can be easily converted to PTMAO polyzwitterions by H_2O_2 oxidation. It is found that H_2O_2 is also able to quickly zwitterionize surface-enriched PDMAEMA chains of nanoporous block polymers of PDMAEMA-*b*-PS prepared by selective swelling-induced pore generation. Longer oxidation leads to lower zeta potentials and WCAs, verifying the enhanced hydrophilicity and the overall electric neutrality of the PTMAO-zwitterionized surface. Water permeance and BSA rejection of the membranes can be tuned by changing the swelling and oxidizing parameters. Because of the presence of PTMAO on the membrane surface, the H_2O_2-zwitterionized PDMAEMA-*b*-PS membranes exhibit ultralow adsorption to both positively and negatively charged proteins and present flux recovery as high as 97% upon dynamic BSA fouling, superior to the fouling-resistant membranes prepared by other methods. This study demonstrates the great potential of the newly discovered PTMAO zwitterions in the membrane field and contributes an easy and reliable approach to diminish membrane fouling.

■ ASSOCIATED CONTENT

Supporting Information

The Supporting Information is available free of charge at https://pubs.acs.org/doi/10.1021/acs.macromol.1c00307.

SEM images; film thickness; XPS spectrum; fouling resistance data; and antifouling performance comparison (PDF)

■ AUTHOR INFORMATION

Corresponding Authors

Jiemei Zhou − *State Key Laboratory of Materials-Oriented Chemical Engineering, College of Chemical Engineering, Nanjing Tech University, Nanjing 211816, Jiangsu, P. R. China*; Email: zhoujm@njtech.edu.cn; Fax: 0086-25-8317 2292

Yong Wang − *State Key Laboratory of Materials-Oriented Chemical Engineering, College of Chemical Engineering, Nanjing Tech University, Nanjing 211816, Jiangsu, P. R. China*; orcid.org/0000-0002-8653-514X; Email: yongwang@njtech.edu.cn

Authors

Chenxu Zhang − *State Key Laboratory of Materials-Oriented Chemical Engineering, College of Chemical Engineering, Nanjing Tech University, Nanjing 211816, Jiangsu, P. R. China*

Xiangyue Ye − *State Key Laboratory of Materials-Oriented Chemical Engineering, College of Chemical Engineering, Nanjing Tech University, Nanjing 211816, Jiangsu, P. R. China*

Zhuo Li − *State Key Laboratory of Materials-Oriented Chemical Engineering, College of Chemical Engineering, Nanjing Tech University, Nanjing 211816, Jiangsu, P. R. China*

Complete contact information is available at: https://pubs.acs.org/10.1021/acs.macromol.1c00307

Notes

The authors declare no competing financial interest.

■ ACKNOWLEDGMENTS

Financial support from the National Natural Science Foundation of China (21908095, 21825803) and the Natural Science Foundation of Jiangsu Province (BK20190671) is gratefully acknowledged.

■ REFERENCES

(1) Park, H. B.; Kamcev, J.; Robeson, L. M.; Elimelech, M.; Freeman, B. D. Maximizing the Right Stuff: The Trade-off between Membrane Permeability and Selectivity. *Science* **2017**, *356*, No. eaab0530.

(2) Wu, J.; Xu, F.; Li, S.; Ma, P.; Zhang, X.; Liu, Q.; Fu, R.; Wu, D. Porous Polymers as Multifunctional Material Platforms toward Task-Specific Applications. *Adv. Mater.* **2019**, *31*, 1802922.
(3) Nunes, S. P. Block Copolymer Membranes for Aqueous Solution Applications. *Macromolecules* **2016**, *49*, 2905−2916.
(4) She, Q.; Wang, R.; Fane, A. G.; Tang, C. Y. Membrane Fouling in Osmotically Driven Membrane Processes: A Review. *J. Membr. Sci.* **2016**, *499*, 201−233.
(5) Lichter, J. A.; Van Vliet, K. J.; Rubner, M. F. Design of Antibacterial Surfaces and Interfaces: Polyelectrolyte Multilayers as a Multifunctional Platform. *Macromolecules* **2009**, *42*, 8573−8586.
(6) Zhang, H.; He, Q.; Luo, J.; Wan, Y.; Darling, S. B. Sharpening Nanofiltration: Strategies for Enhanced Membrane Selectivity. *ACS Appl. Mater. Interfaces* **2020**, *12*, 39948−39966.
(7) Weber, M.; Julbe, A.; Ayral, A.; Miele, P.; Bechelany, M. Atomic Layer Deposition for Membranes: Basics, Challenges, and Opportunities. *Chem. Mater.* **2018**, *30*, 7368−7390.
(8) Wei, Q.; Becherer, T.; Angioletti-Uberti, S.; Dzubiella, J.; Wischke, C.; Neffe, A. T.; Lendlein, A.; Ballauff, M.; Haag, R. Protein Interactions with Polymer Coatings and Biomaterials. *Angew. Chem., Int. Ed.* **2014**, *53*, 8004−8031.
(9) Chang, Y.; Shu, S.-H.; Shih, Y.-J.; Chu, C.-W.; Ruaan, R.-C.; Chen, W.-Y. Hemocompatible Mixed-charge Copolymer Brushes of Pseudozwitterionic Surfaces Resistant to Nonspecific Plasma Protein Fouling. *Langmuir* **2010**, *26*, 3522−3530.
(10) Chen, W.; Su, Y.; Peng, J.; Zhao, X.; Jiang, Z.; Dong, Y.; Zhang, Y.; Liang, Y.; Liu, J. Efficient Wastewater Treatment by Membranes through Constructing Tunable Antifouling Membrane Surfaces. *Environ. Sci. Technol.* **2011**, *45*, 6545−6552.
(11) Jiang, J.; Zhu, L.; Zhu, L.; Zhang, H.; Zhu, B.; Xu, Y. Antifouling and Antimicrobial Polymer Membranes Based on Bioinspired Polydopamine and Strong Hydrogen-bonded Poly(N-vinyl pyrrolidone). *ACS Appl. Mater. Interfaces* **2013**, *5*, 12895−12904.
(12) Chen, S.; Li, L.; Zhao, C.; Zheng, J. Surface hydration: Principles and Applications toward Low-fouling/Nonfouling Biomaterials. *Polymer* **2010**, *51*, 5283−5293.
(13) Darling, S. B. Perspective: Interfacial materials at the interface of energy and water. *J. Appl. Phys.* **2018**, *124*, 030901.
(14) Mi, L.; Jiang, S. Integrated Antimicrobial and Nonfouling Zwitterionic Polymers. *Angew. Chem., Int. Ed.* **2014**, *53*, 1746−1754.
(15) Delgado, J. D.; Schlenoff, J. B. Static and Dynamic Solution Behavior of a Polyzwitterion Using a Hofmeister Salt Series. *Macromolecules* **2017**, *50*, 4454−4464.
(16) Schönemann, E.; Laschewsky, A.; Rosenhahn, A. Exploring the Long-Term Hydrolytic Behavior of Zwitterionic Polymethacrylates and Polymethacrylamides. *Polymers* **2018**, *10*, 639−662.
(17) Brown, R. H.; Duncan, A. J.; Choi, J.-H.; Park, J. K.; Wu, T.; Leo, D. J.; Winey, K. I.; Moore, R. B.; Long, T. E. Effect of Ionic Liquid on Mechanical Properties and Morphology of Zwitterionic Copolymer Membranes. *Macromolecules* **2010**, *43*, 790−796.
(18) Akamatsu, K.; Mitsumori, K.; Han, F.; Nakao, S.-i. Fouling-Free Membranes Obtained by Facile Surface Modification of Commercially Available Membranes Using the Dynamic Forming Method. *Ind. Eng. Chem. Res.* **2011**, *50*, 12281−12284.
(19) Zhao, J.; Shi, Q.; Luan, S.; Song, L.; Yang, H.; Stagnaro, P.; Yin, J. Polypropylene Non-woven Fabric Membrane via Surface Modification with Biomimetic Phosphorylcholine in Ce(IV)/HNO_3 Redox System. *Mater. Sci. Eng., C* **2012**, *32*, 1785−1789.
(20) Hildebrand, V.; Laschewsky, A.; Päch, M.; Müller-Buschbaum, P.; Papadakis, C. M. Effect of the Zwitterion Structure on the Thermo-Responsive Behaviour of Poly(sulfobetaine methacrylates). *Polym. Chem.* **2017**, *8*, 310−322.
(21) Shao, Q.; Jiang, S. Effect of Carbon Spacer Length on Zwitterionic Carboxybetaines. *J. Phys. Chem. B* **2013**, *117*, 1357−1366.
(22) Li, B.; Jain, P.; Ma, J.; Smith, J. K.; Yuan, Z.; Hung, H.-C.; He, Y.; Lin, X.; Wu, K.; Pfaendtner, J.; Jiang, S. Trimethylamine *N*-oxide-derived Zwitterionic Polymers: A new Class of Ultralow Fouling Bioinspired Materials. *Sci. Adv.* **2019**, *5*, No. eaaw9562.
(23) Keating, J. J.; Imbrogno, J.; Belfort, G. Polymer Brushes for Membrane Separations: A Review. *ACS Appl. Mater. Interfaces* **2016**, *8*, 28383−28399.
(24) Miyano, T.; Matsuura, T.; Sourirajan, S. Effect of Polyvinylpyrrolidone Additive on the Pore-Size and the Pore-Size Distribution of Polyethersulfone (Victrex) Membranes. *Chem. Eng. Commun.* **1993**, *119*, 23−39.
(25) Rana, D.; Matsuura, T. Surface Modifications for Antifouling Membranes. *Chem. Rev.* **2010**, *110*, 2448−2471.
(26) Zhou, J.; Wang, Y. Selective Swelling of Block Copolymers: An Upscalable Greener Process to Ultrafiltration Membranes? *Macromolecules* **2020**, *53*, 5−17.
(27) Wang, Y.; Li, F. An Emerging Pore-Making Strategy: Confined Swelling-Induced Pore Generation in Block Copolymer Materials. *Adv. Mater.* **2011**, *23*, 2134−2148.
(28) Wang, Y. Nondestructive Creation of Ordered Nanopores by Selective Swelling of Block Copolymers: Toward Homoporous Membranes. *Acc. Chem. Res.* **2016**, *49*, 1401−1408.
(29) Zhong, D.; Wang, Z.; Lan, Q.; Wang, Y. Selective Swelling of Block Copolymer Ultrafiltration Membranes for Enhanced Water Permeability and Fouling Resistance. *J. Membr. Sci.* **2018**, *558*, 106−112.
(30) Yang, H.; Zhou, J.; Wang, Z.; Shi, X.; Wang, Y. Selective Swelling of Polysulfone/poly(ethylene glycol) Block Copolymer towards Fouling-resistant Ultrafiltration Membranes. *Chin. J. Chem. Eng.* **2020**, *28*, 98−103.
(31) Yang, H.; Wang, Z.; Lan, Q.; Wang, Y. Antifouling Ultrafiltration Membranes by Selective Swelling of Polystyrene/poly(ethylene oxide) Block Copolymers. *J. Membr. Sci.* **2017**, *542*, 226−232.
(32) Zhang, C.; Yin, C.; Wang, Y.; Zhou, J.; Wang, Y. Simultaneous Zwitterionization and Selective Swelling-induced Pore Generation of Block Copolymers for Antifouling Ultrafiltration Membranes. *J. Membr. Sci.* **2020**, *599*, 117833.
(33) Zhou, J.; Zhang, C.; Wang, Y. Nanoporous Block Copolymer Membranes Immobilized with Gold Nanoparticles for Continuous Flow Catalysis. *Polym. Chem.* **2019**, *10*, 1642−1649.
(34) Wei, Y.; Zeng, Q.; Huang, J.; Guo, X.; Wang, L.; Wang, L. Preparation of Gas-Responsive Imprinting Hydrogel and Their Gas-Driven Switchable Affinity for Target Protein Recognition. *ACS Appl. Mater. Interfaces* **2020**, *12*, 24363−24369.
(35) Koufakis, E.; Manouras, T.; Anastasiadis, S. H.; Vamvakaki, M. Film Properties and Antimicrobial Efficacy of Quaternized PDMAEMA Brushes: Short vs Long Alkyl Chain Length. *Langmuir* **2020**, *36*, 3482−3493.
(36) Stubbs, C.; Congdon, T.; Davis, J.; Lester, D.; Richards, S.-J.; Gibson, M. I. High-Throughput Tertiary Amine Deoxygenated Photopolymerizations for Synthesizing Polymer Libraries. *Macromolecules* **2019**, *52*, 7603−7612.
(37) Larini, L.; Shea, J.-E. Double Resolution Model for Studying TMAO/Water Effective Interactions. *J. Phys. Chem. B* **2013**, *117*, 13268−13277.
(38) Dobrzanska, D. A.; Cooper, A. L.; Dowson, C. G.; Evans, S. D.; Fox, D. J.; Johnson, B. R.; Biggs, C. I.; Randev, R. K.; Stec, H. M.; Taylor, P. C.; Marsh, A. Oxidation of Tertiary Amine-Derivatized Surfaces to Control Protein Adhesion. *Langmuir* **2013**, *29*, 2961−2970.
(39) Shi, X.; Wang, X.; Wang, Y.; Wang, Y. Producing Nanoporosities in Block Copolymers within 30 s by Microwave-Boosted Selective Swelling. *Macromolecules* **2020**, *53*, 3619−3626.
(40) Bengani-Lutz, P.; Converse, E.; Cebe, P.; Asatekin, A. Self-Assembling Zwitterionic Copolymers as Membrane Selective Layers with Excellent Fouling Resistance: Effect of Zwitterion Chemistry. *ACS Appl. Mater. Interfaces* **2017**, *9*, 20859−20872.
(41) Yang, X.; Sun, H.; Pal, A.; Bai, Y.; Shao, L. Biomimetic Silicification on Membrane Surface for Highly Efficient Treatments of

https://doi.org/10.1021/acs.macromol.1c00307
Macromolecules 2021, 54, 4236−4245

Both Oil-in-Water Emulsion and Protein Wastewater. *ACS Appl. Mater. Interfaces* **2018**, *10*, 29982−29991.
(42) Zhang, H.; He, Q.; Luo, J.; Wan, Y.; Darling, S. B. Sharpening Nanofiltration: Strategies for Enhanced Membrane Selectivity. *ACS Appl. Mater. Interfaces* **2020**, *12*, 39948−39966.

https://doi.org/10.1021/acs.macromol.1c00307
Macromolecules 2021, 54, 4236−4245